ACS Catalysis

Research Article

pubs.acs.org/acscatalysis

Dopant Effect of Barium Zirconate-Based Perovskite-Type Catalysts for the Intermediate-Temperature Reverse Water Gas Shift Reaction

Dae Han Kim,[†] Jae Layng Park,[§] Eun Ji Park,[†] Young Dok Kim,*[,†,‡] and Sunghyun Uhm*[,§]

[†]Department of Chemistry, Sungkyunkwan University, Suwon 440-746, Korea

[‡]Biorefinery Research Group, Korean Research Institute of Chemical Technology, Daejeon 306-600, Korea

[§]Advanced Materials and Processing Center, Institute for Advanced Engineering, Yongin 449-863, Korea

ABSTRACT: The reverse water gas shift (RWGS) reaction catalyzed by barium zirconate-based perovskite-type catalysts doped with Y, Zn, and Ce was investigated in terms of activities and chemical stabilities of various catalysts. All of the catalysts showed stable performances for the RWGS reaction at 600 °C for 5 h, and in particular, the $BaZr_{0.8}Y_{0.16}Zn_{0.04}O_3$ (BZYZ) catalyst showed an outstanding activity with an average CO_2 conversion of 37.5% and a CO selectivity of 97%. Insertion of additional Ce into the BZYZ structure did not have any positive effect on catalytic activity for the RWGS reaction, even though the ionic conductivity of BZYZ was improved by Ce insertion.

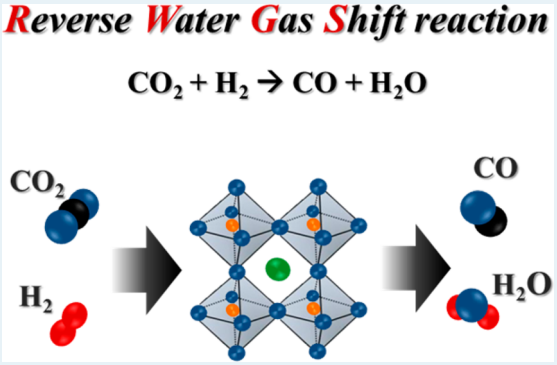

KEYWORDS: *reverse water gas shift reaction, CO_2, barium zirconates, dopant, perovskite*

1. INTRODUCTION

Various strategies of carbon capture and sequestration (CCS) at large emission sources such as power plants are needed to decrease the level of accumulation of CO_2 in the atmosphere. It is important to note that evaluation of the impact of transferring large amounts of CO_2 into uncontrolled underground storage is very difficult. Instead, utilization of CO_2 before storage as a feedstock to produce a myriad of industrially relevant reaction precursors and organic materials represents a potentially sustainable and long-term resource.[1−4]

With the aim of effectively using CO_2, synthesis gas production by the stoichiometric reverse water gas shift (RWGS) reaction, which converts atmospheric CO_2 and H_2 to renewable energy sources, has been proposed (eq 1).[5−8]

$$CO_2 + H_2 \leftrightarrow CO + H_2O \quad H^\circ = 41.2\ \text{kJ/mol} \qquad (1)$$

Because of the reversibility of the RWGS reaction, its maximal conversion and selectivity are typically governed by a thermodynamic equilibrium, and the conversion of CO_2 to CO depends on reaction temperature. Although reactions at higher temperatures are effective for obtaining a higher level of conversion due to the endothermic nature of this reaction, a low-temperature process with less energy consumption is highly desirable for the following reason. The high-temperature operation of the RWGS reaction makes the cascade utilization of thermal energy more difficult.[8] It should be mentioned that the water formed in the RWGS reaction must be removed, because otherwise it deactivates the catalytic activity of subsequent reactions, and it is thus convenient to have a process scheme based on multistage reactors with an intermediate water separation stage prior to methanol synthesis or Fischer−Tropsch reactions.

In the field of heterogeneous catalysis, it has been found over the years that metal catalysts dispersed on ion-conducting supports have activities for many catalytic reactions, including the RWGS reaction, much higher than those of the same metal catalysts dispersed on inert supports.[9] This has led to gradual substitution of the classical nonconducting supports (SiO_2 and Al_2O_3) with those exhibiting significant ionic or mixed ionic−electronic conductivity (such as doped ZrO_2, TiO_2, and CeO_2).[10−13]

Mixed metal oxides with the ABO_3 perovskite structure can be considered as promising ceramic materials for catalytic applications when they are used as supports for rare-earth and 3d transition metals.[10] This family of oxides has already been widely used as electrodes and electrolytes in heterogeneous catalysis and solid-state electrochemistry. The catalytic and electrocatalytic properties of perovskites can be tuned by varying the nature of A and B cations and/or by insertion of dopants into the structure, which can lead to an increase in the structural defect density as a consequence of stabilization of unusual oxidation states by B components. The attractive attributes of perovskite oxides for catalytic applications include the high mobility of oxygen and its ability to stabilize unusual cationic oxidation states, together with the thermal stability at high temperatures.[14−17] The alkaline, alkaline-earth, and rare-

Received: April 10, 2014
Revised: July 1, 2014
Published: July 30, 2014

 © 2014 American Chemical Society dx.doi.org/10.1021/cs500476e | ACS Catal. 2014, 4, 3117−3122

earth metals are generally employed as promoters, and they are involved in altering the acid−base property of the catalyst, improving the dispersion of active species, and increasing the strength of the interaction of active species and support.

In this study, we report the RWGS reaction activities of alkaline-earth-based perovskite-type oxide catalysts, barium zirconates ($BaZrO_3$), which show a high affinity for CO_2.[18] In addition, the effects of compositional modification of the catalysts by additional dopants on catalytic activity are discussed. Catalytic properties of the $BaCe_xZr_{0.8-x}Y_{0.16}Zn_{0.04}O_3$ (BCZYZ*x*) catalysts in the RWGS reaction at 600 °C were evaluated in terms of catalytic activity and proton conductivity, which are expected to be modulated by the addition of Ce.

The role of Ba in $BaZrO_3$ catalysts was known to increase the density of basic sites, which provide CO_2 adsorption sites.[17] Also, with an optimal combination of a high oxygen vacancy and basicity induced by Ba, the CO_2 reduction process of the catalytic cycle was accelerated. Y was added to promote oxygen vacancy and proton incorporation, and Y_2O_3 is a thermally and chemically stable compound that can maintain the cubic structure stably even at high temperatures without exhibiting valence variation of rare-earth ions among several cubic-type rare-earth oxides.[13] ZnO was also added to improve the dispersion and redox properties of catalysts.

2. EXPERIMENTAL DETAILS

2.1. Sample Preparation. The $BaCe_xZr_{0.8-x}Y_{0.16}Zn_{0.04}O_3$ (BCZYZ*x*) samples were prepared by a conventional solid-state reaction method. Starting materials were $BaCO_3$ (Aldrich, 99.9%), ZrO_2 (Aldrich, 99.9%), CeO_2 (Aldrich, 99.9%), ZnO (Aldrich, 99.7%), Y_2O_3 (SRX, 99.99%), and acetone. All materials were ground together in acetone, dried at 110 °C, and then calcined in air at 1200 °C for 5 h. Finally, the calcined products were crushed into uniform powders by attrition milling. In this work, Y-doped $BaZr_{0.8}Y_{0.2}O_3$ (BZY), Y, Zn-doped $BaZr_{0.8}Y_{0.16}Zn_{0.04}O_3$ (BZYZ), and BCZYZ*x* with three different amounts of Ce dopants were synthesized.

2.2. RWGS Reaction. Catalytic RWGS reactions were conducted in a continuous flow quartz reactor (31 mm internal diameter and 530 mm length) at atmospheric pressure; 0.5 g of each catalyst was placed vertically in a fixed-bed reactor (Figure 1). The sample was pretreated at 700 °C for 3 h with a flow of dry air (30 mL/min), and then the surface of the sample was subsequently exposed to H_2 (30 mL/min) at 600 °C for 6 h before the RWhGS reaction. After pretreatment, a reagent gas mixture (1:1 CO_2:H_2 ratio) was fed into the reactor with a fixed total flow of 20 mL/min at room temperature. The mass flow of the reagent gas mixture was not influenced by the existence of the catalysts in a fixed-bed reactor.

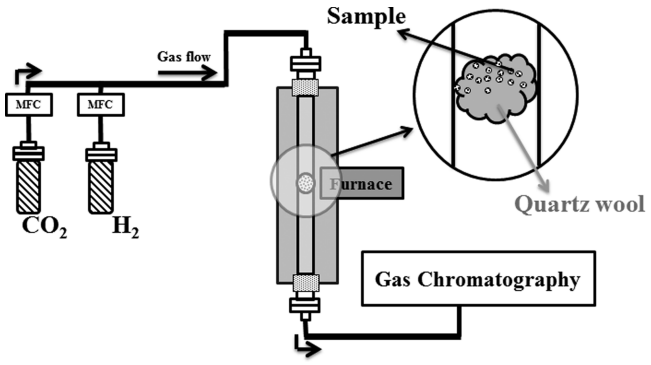

Figure 1. Schematic image of the catalytic activity test setup for the RWGS reaction.

After the flow of the reagent gas mixture was stabilized, the temperature of the reactor was increased to 600 °C at a constant heating rate of 5 °C/min. The temperature was maintained at 600 °C for 320 min, and the relative concentrations of CO_2, H_2, and CO were monitored using an online gas chromatograph (Hewlett Packard, HP6890) equipped with a fused silica capillary column (SUPELCO, Carboxen 1010 PLOT, 30 m × 0.32 mm), a thermal conductivity detector (TCD), and a flame ionization detector (FID). High-purity N_2 (99.999%) was used as a carrier gas for the gas chromatography column, and the temperature of the reactor was monitored with a K-type thermocouple.

2.3. Sample Characterization. The morphological images and elemental compositions of BZY and BCZYZ*x* catalysts were obtained by scanning electron microscopy (SEM) and energy dispersive X-ray spectroscopy (EDX), respectively. The surface area of each sample was determined by the Brunauer−Emmett−Teller (BET) method. The composition and crystallinity of each sample were analyzed by X-ray diffraction (XRD). XRD measurements were performed using an XRD spectrometer (Ultima IV, Rigaku) equipped with a Cu Kα line (λ = 0.15406 nm) X-ray source. The proton conductivity of each sample was measured by a direct current method with a four-point probe setup (Autolab potentiostat/galvanostat, PGSTAT302N). The measurements of pelletized samples were performed in wet 3% H_2 by passing the gas through room-temperature water. The topmost surface composition and chemical state of each catalyst were analyzed by X-ray photoelectron spectroscopy (XPS). XPS measurements were performed in an ultra-high-vacuum (UHV) chamber (base pressure of 5.0×10^{-10} Torr) equipped with a concentric hemispherical analyzer (CHA, PHOIBOS-Has 3500, SPECS) and a dual Al/Mg X-ray source. All XPS spectra were acquired at room temperature using a Mg Kα line (1253.6 eV).

3. RESULTS AND DISCUSSION

Ion-conducting ceramics are new and promising catalyst supports of finely dispersed and stabilized metallic nanoparticles for the improvement of their performance. Spillover of ions from the ceramic electrolyte materials onto the metal catalyst (or electrode) surface is a reversible process. It can affect the (electro) catalytic kinetics, and importantly, it is a crucial factor for determining the catalytic properties of metals in contact with electrolyte supports. In this regard, several proton-conducting ceramics have been investigated in heterogeneous catalysis.[18−21] Furthermore, it has been well reported that ceria-supported catalysts were active for the RWGS reaction because of its good oxygen-exchange property[22] in conjunction with the characteristics of ionic conductivity. Ceria support is a versatile oxygen exchanger, having an outstanding redox property and creating an oxygen vacancy on the surface. It was determined that ionic conductivity is directly related to the diffusion of an oxygen vacancy on a catalyst surface.[23] This redox property of a catalyst has also been considered to be one of the important factors for determining the catalytic activity of the RWGS reaction[7] because the catalyst surface is repeatedly oxidized and reduced during the reaction by CO_2 and H_2 reagents, respectively.

Proton conductivities of $BaCe_xZr_{0.8-x}Y_{0.16}Zn_{0.04}O_3$ (BCZYZ*x*) catalysts at two different temperatures (600 and

dx.doi.org/10.1021/cs500476e | ACS Catal. 2014, 4, 3117−3122

700 °C) were measured, and the results are shown in Figure 2. It was obvious that proton conductivity increased with an

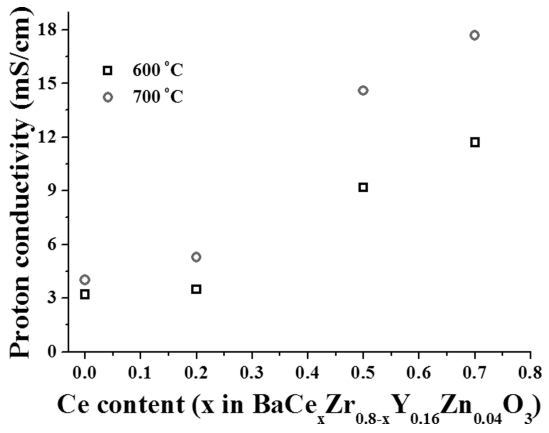

Figure 2. Proton conductivity results of $BaCe_xZr_{0.8-x}Y_{0.16}Zn_{0.04}O_3$ (BCZYZ*x*) catalysts at 600 and 700 °C.

increase in Ce content. In particular, the increase in proton conductivity by insertion of Ce was pronounced at both temperatures as *x* became larger than 0.2. The values of proton conductivities determined here are in a good agreement with those of previous studies.[24,25]

Catalytic performances of $BaZr_{0.8}Y_{0.2}O_3$ (BZY) and BCZYZ*x* catalysts for the RWGS reaction were measured as a function of time (Figure 3), and the results are summarized in Table 1. All

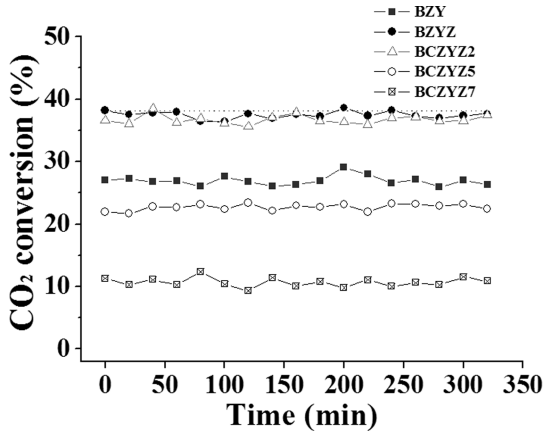

Figure 3. Results of catalytic RWGS reactions over $BaZr_{0.8}Y_{0.2}O_3$ (BZY) and $BaCe_xZr_{0.8-x}Y_{0.16}Zn_{0.04}O_3$ (BCZYZ*x*) catalysts at 600 °C are compared. CO_2 conversion is plotted as a function of reaction time for ∼5 h at 600 °C. CO_2 conversion in the equilibrium state at 600 °C is shown in as dashed gray line.

Table 1. Results of the RWGS Reaction at 600 °C over $BaZr_{0.8}Y_{0.2}O_3$ (BZY), $BaZr_{0.8}Y_{0.16}Zn_{0.04}O_3$ (BZYZ), and $BaCe_xZr_{0.8-x}Y_{0.16}Zn_{0.04}O_3$ (BCZYZ*x*) Catalysts

catalyst	CO_2 conversion (%)	CO selectivity
BZY ($BaZr_{0.8}Y_{0.2}O_3$)	26.7	0.93
BZYZ ($BaZr_{0.8}Y_{0.16}Zn_{0.04}O_3$)	37.5	0.97
BCZYZ2 ($BaCe_{0.2}Zr_{0.6}Y_{0.16}Zn_{0.04}O_3$)	36.3	0.94
BCZYC5 ($BaCe_{0.5}Zr_{0.3}Y_{0.16}Zn_{0.04}O_3$)	22.3	0.92
BCZYC7 ($BaCe_{0.7}Zr_{0.1}Y_{0.16}Zn_{0.04}O_3$)	10.8	0.74

catalysts showed stable catalytic activities for ∼5 h. Among the catalysts studied here, $BaZr_{0.8}Y_{0.16}Zn_{0.04}O_3$ (BZYZ) showed the highest CO_2 conversion of 37.5%, which was almost identical to the thermodynamic equilibrium conversion for the RWGS reaction at 600 °C and atmospheric pressure. According to the previous study of Saito's group,[18] barium zirconate ($BaZrO_3$) showed a relatively low catalytic activity for the RWGS reaction under 700 °C without any Zr-site substitution. As shown in Figure 3, BZY with only Y (as Y_2O_3) doping showed a relatively low catalytic activity, whereas the catalytic activity was significantly enhanced by Zn doping.

With regard to the CO selectivity, although the ideal CO selectivity should be 1 in the RWGS reaction (i.e., all converted CO_2 should yield CO), some side reactions could take place, resulting in a CO selectivity of <1 (0.97 for BZYZ). This result could be associated with the fact that doped Zr catalysts are well-known to have a catalytic activity for hydrocarbon synthesis,[26] i.e., Fischer−Tropsch (FT) synthesis (eq 2).

$$CO(g) + H_2(g) \rightarrow -CH_2-(g) + H_2O(g)$$
$$\Delta H_{573K} = -166\ \text{kJ/mol} \quad (2)$$

Data in Table 1 show that BZYZ with a CO selectivity of 0.97 was the best catalyst in terms of not only total conversion but also selectivity.

Cu-based catalysts have been widely studied in the RWGS reaction, and they showed CO_2 conversions of ∼20% at 600 °C.[6,27] Ce-based catalysts were also active in the RWGS reaction; e.g., Ni/CeO_2 (2 wt % Ni) showed a CO_2 conversion of ∼35% and a CO selectivity of ∼0.99 for the RWGS reaction at 600 °C for 9 h.[28] Although it is hard to directly compare activities of the catalysts of previous studies with that of the BZYZ catalyst because of dissimilar experimental parameters, it is obvious that BZYZ catalysts with a CO_2 conversion of 37.5% in our study are highly active for the RWGS reaction and chemically stable (Figure 3). It was also determined that the BZYZ catalyst was very stable even at 800 °C for 10 h during the RWGS reaction with a CO_2 conversion of 44.9% and a CO selectivity of 0.94 (data not shown).

With regard to Ce doping, introduction of the smallest amount of Ce into the BZYZ catalyst [$BaCe_{0.2}Zr_{0.6}Y_{0.16}Zn_{0.04}O_3$ (BCZYZ2)] structure had almost no effect on the catalytic activity for the RWGS reaction. The CO_2 conversion of the BCZYZ*x* catalyst gradually decreased as the *x* representing the Ce proportion exceeded 0.2, in spite of the improvement in proton conductivity. On the basis of the results in Figure 3 and Table 1, one can conclude that codoping of Y and Zn (as ZnO) was a highly effective way to improve the catalytic activity for the RWGS reaction, whereas additional doping of Ce in BZYZ catalysts was not.

To clarify why the introduction of Ce did not have any positive effect on the catalytic activity for the RWGS reaction, we conducted physicochemical analyses of the catalysts. Elemental compositions of as-prepared catalysts were analyzed by EDX, whereas surface areas and mean particle sizes were determined by BET and SEM, respectively (Table 2). We also calculated catalytic activities normalized by the surface area of the respective catalyst (Table 2). The surface area-normalized activity and Ce doping did not show a clear correlation; however, it was obvious that that the particle size of the $BaZrO_3$ catalyst was increased with Ce doping. As one can see in SEM images of BZY, BZYZ, and BCZYZ2 catalysts (Figure 4a,c,e), mean particle sizes of the catalysts were in the range of 200−

dx.doi.org/10.1021/cs500476e | ACS Catal. 2014, 4, 3117−3122

Table 2. Elemental Compositions, Surface Areas, Mean Particle Sizes, and Normalized CO_2 Conversions of $BaZr_{0.8}Y_{0.2}O_3$ (BZY), $BaZr_{0.8}Y_{0.16}Zn_{0.04}O_3$ (BZYZ), and $BaCe_xZr_{0.8-x}Y_{0.16}Zn_{0.04}O_3$ (BCZYZ*x*) Catalysts

			BCZYZ*x* ($BaCe_xZr_{0.8-x}Y_{0.16}Zn_{0.04}O_3$)		
	BZY ($BaZr_{0.8}Y_{0.2}O_3$)	BZYZ ($BaZr_{0.8}Y_{0.16}Zn_{0.04}O_3$)	BCZYZ2	BCZYZ5	BCZYZ7
elemental composition (atom %)					
Ba	18.3	15.3	23.5	17.3	18.7
Ce	–	–	4.7	8.3	12.5
Zr	15.1	11.8	12.0	5.0	1.9
Y	2.7	2.4	3.2	2.7	2.6
Zn	–	1.4	1.2	1.0	1.8
surface area (m^2/g)	13.4	12.1	13.6	7.1	7.2
particle size (μm)	0.15	0.16	0.25	0.24	0.23
surface area-normalized CO_2 conversion (%)	3.99	6.20	5.34	6.28	3.00

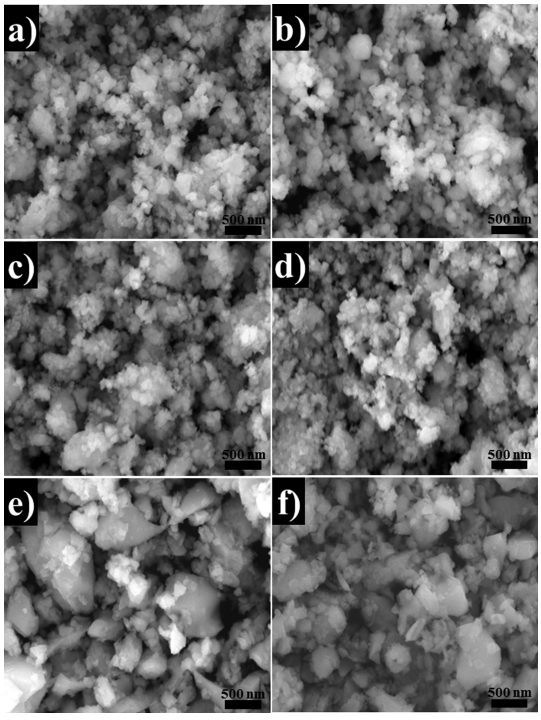

Figure 4. SEM images of $BaZr_{0.8}Y_{0.2}O_3$ (BZY) (a and b), $BaZr_{0.8}Y_{0.16}Zn_{0.04}O_3$ (BZYZ) (c and d), and $BaCe_{0.2}Zr_{0.6}Y_{0.16}Zn_{0.04}O_3$ (BCZYZ2) (e and f) catalysts before and after the RWGS reaction, respectively.

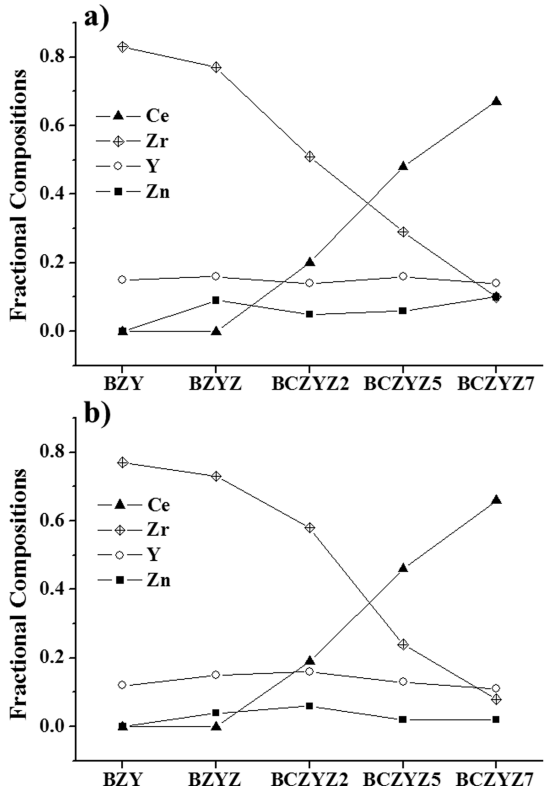

Figure 5. Elemental compositions of $BaZr_{0.8}Y_{0.2}O_3$ (BZY), $BaZr_{0.8}Y_{0.16}Zn_{0.04}O_3$ (BZYZ), and $BaCe_xZr_{0.8-x}Y_{0.16}Zn_{0.04}O_3$ (BCZYZ*x*) catalysts (a) before and (b) after the RWGS reaction.

1000 nm, and the population of particles with larger sizes (Table 2) became more abundant as Ce was introduced. It was also found that the surface morphologies of BZY and BCZYZ*x* catalysts were not much changed after the RWGS reaction at 600 °C (Figure 4b,d,f).

We also analyzed changes in the elemental compositions of each catalyst after the RWGS reaction (Figure 5). It is worth mentioning that all the elemental compositions in Figure 5 have been normalized by the Ba amount of the respective catalyst. Here, we found that the average values of the fractional composition of Zn in BZYZ, BCZYZ5, and BCZYZ7 catalysts were significantly decreased after the RWGS reaction. However, there was no noticeable change in the fractional compositions of other elements (Ce, Zr, and Y).

Before the RWGS reaction, we confirmed that all of the catalysts showed the major peaks in XRD, being consistent with a single perovskite phase of BZY, and the spacing between lattice planes of BZY was gradually expanded by the insertion of Ce (data not shown). Figure 6 shows the XRD data of BZY, BZYZ, and BCZYZ*x* catalysts after the RWGS reaction at 600 °C for 5 h. Here, there was no large difference in the XRD patterns of BZY, BZYZ, and BCZYZ2 samples after the RWGS reaction: BZY lattice structures were still maintained after the RWGS reaction.[29] However, BCZYZ5 and BCZYZ7, Ce-rich catalysts, showed much different XRD spectra after the RWGS reaction. It was determined that the peaks corresponding to the lattice planes of $BaCO_3$ appeared instead of BZY lattice planes,[29] meaning that the BCZYZ5 and BCZYZ7 catalysts were chemically unstable under the RWGS reaction condition. Considering the stable performances of all catalysts, the collapse of the BZY crystal structure shown in BCZYZ5 and BCZYZ7 catalysts could take place during the pretreatment process. These results might be not consistent with those of previous studies.[24,25] Such discrepancies between our work and previous works could come from the fact that all samples in this

dx.doi.org/10.1021/cs500476e | ACS Catal. 2014, 4, 3117−3122

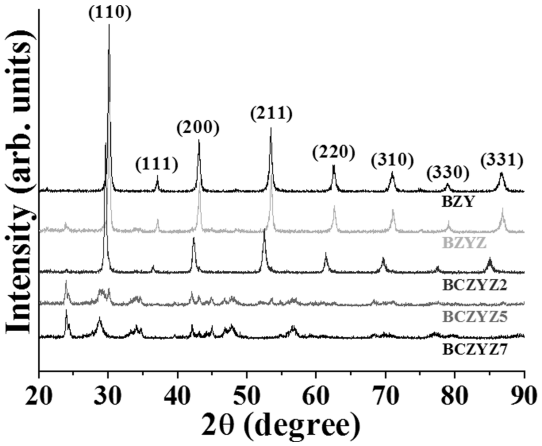

Figure 6. XRD spectra of $BaZr_{0.8}Y_{0.2}O_3$ (BZY), $BaZr_{0.8}Y_{0.16}Zn_{0.04}O_3$ (BZYZ), and $BaCe_xZr_{0.8-x}Y_{0.16}Zn_{0.04}O_3$ (BCZYZ*x*) catalysts after the RWGS reaction.

study were pre-exposed to air and H_2 at elevated temperatures, whereas samples in the references were exposed to only pure CO_2.

The surface chemical states of BZY, BZYZ, and BCZYZ*x* catalysts were analyzed by XPS before and after the RWGS reaction at 600 °C. All core-level XPS spectra of each catalyst were normalized by the respective Ba $3d_{5/2}$ core-level peak with a binding energy of 779.9 eV. Figure 7 shows the Ce 3d and Zn 2p core-level XPS spectra that were significantly changed after the RWGS reaction at 600 °C.[30] Before the RWGS reaction, it was determined that the Ce dopant in the topmost surface layer existed in at least two different oxidation states with CeO_2 and reduced Ce, and the largest amount of Ce was observed on the BCZYZ7 catalyst surface. After the reaction, a noticeable change in the amount of Ce dopant in the surface layer was observed on the BCZYZ7 catalyst: the amount of Ce dopant in the surface layer of the BCZYZ7 catalyst was drastically decreased, and all BCZYZ*x* catalysts showed similar amounts of Ce on the catalysts (Figure 7a,b). This result is not consistent with EDX data of BCZYZ*x* catalysts after the RWGS reaction (Figure 5b), which is due to dissimilar detection limits of different analysis methods (XPS is much more surface-sensitive than EDX). One can conclude that the Ce dopant in the surface topmost layer was not directly related to the change in catalytic activities of BCZYZ*x* catalysts for the RWGS reaction because the amounts of Ce dopant on the catalyst surface were almost the same regardless of the Ce compositions of the BCZYZ*x* catalysts.

In Zn 2p core-level XPS spectra, the intensity of the Zn $2p_{3/2}$ peak centered at 1021.4 eV was decreased after the RWGS reaction by 19.6 and 71.1% for BCZYZ2 and BCZYZ5 catalysts, respectively. The Zn $2p_{3/2}$ peak of the BCZYZ7 catalyst almost

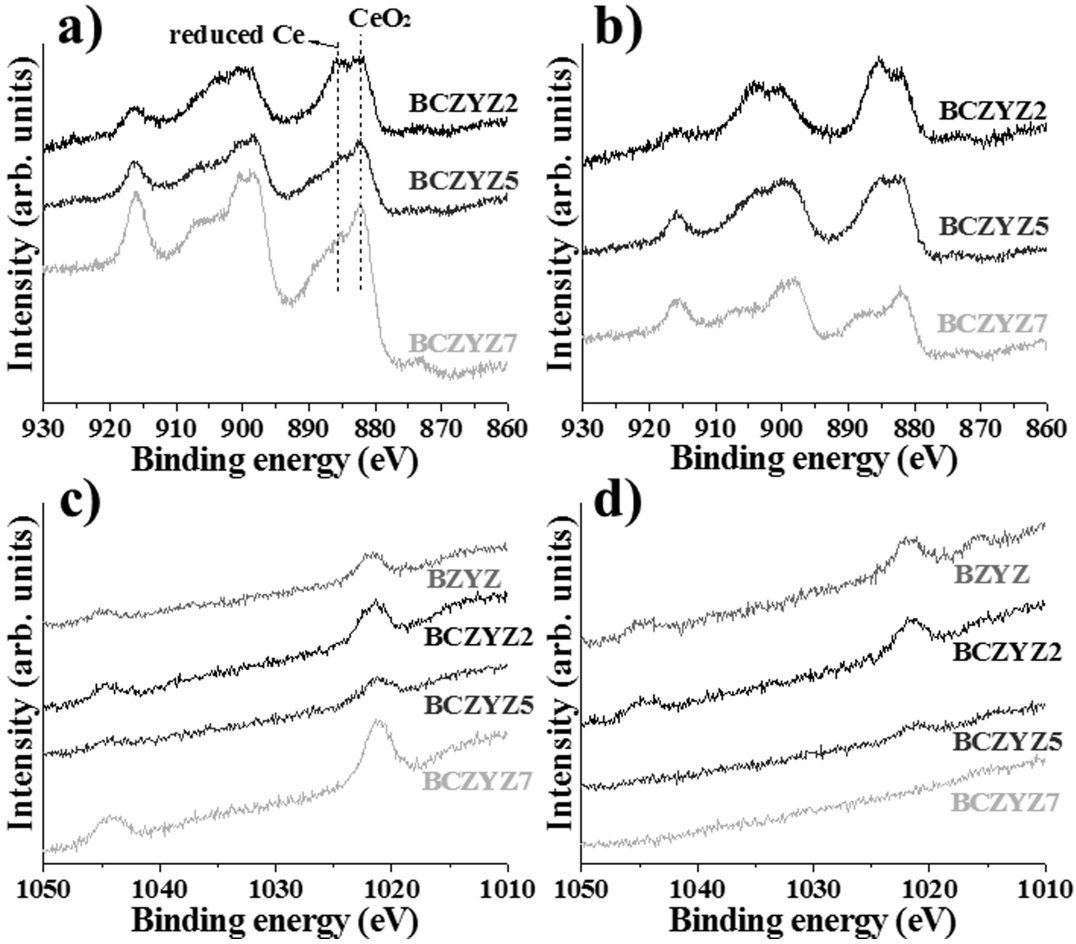

Figure 7. XPS spectra of $BaZr_{0.8}Y_{0.16}Zn_{0.04}O_3$ (BZYZ) and $BaCe_xZr_{0.8-x}Y_{0.16}Zn_{0.04}O_3$ (BCZYZ*x*) catalysts before and after the RWGS reaction. (a and b) XPS spectra of Ce 3d before and after the RWGS reaction, respectively. (c and d) XPS spectra of Zn 2p before and after the RWGS reaction, respectively.

dx.doi.org/10.1021/cs500476e | ACS Catal. 2014, 4, 3117−3122

completely disappeared after the RWGS reaction (Figure 7c,d).[30] A similar tendency was also found in EDX results after the RWGS reaction as shown in Figure 5b: BCZYZ5 and BCZYZ7 catalysts had very small amounts of Zn dopant after the RWGS reaction. This might be caused by vaporization of Zn from the catalyst structure during pretreatment or the RWGS reaction at ~700 °C, and the disappearance of Zn from the catalyst surface became more pronounced with additional Ce doping. Generally, it has been known that ZnO can be relatively easily vaporized and used for the fabrication of a Zn film by the thermal evaporation method.[31]

Considering the XPS data combined with the EDX and XRD results, one can conclude that the poor catalytic activities of Ce-rich catalysts shown in Figure 3 could be due to the development of the Zn-deficient surface structure of the BCZYZ*x* catalyst in the presence of Ce. This could induce collapse of the BZY perovskite structure and decrease the catalytic activity.

4. CONCLUSION

Barium zirconate-based pervoskite-type catalysts were evaluated for the RWGS reaction with different dopants. The Zn- and Y-doped BZYZ catalyst showed an outstanding activity for the RWGS reaction even at an intermediate temperature of 600 °C, while additional introduction of Ce into the BZYZ catalyst caused the appearance of a Zn-deficient surface structure and chemical instability of the catalyst, ultimately decreasing catalytic activity.[20] Both proton conductivity and activity for the RWGS reaction are facilitated by the same type of vacant oxygen site acting as a host; however, we suggest that an increase in the number of oxygen vacancies could decrease the chemical stability of catalysts. Thus, not only the tuning of the elemental composition of the catalyst but also the interaction between the elements in the catalyst during a chemical reaction should be carefully considered.

AUTHOR INFORMATION

Corresponding Authors

*E-mail: ydkim91@skku.edu.

*E-mail: laminat@hanmail.net.

Notes

The authors declare no competing financial interest.

ACKNOWLEDGMENTS

This work was supported by a Korea CCS R&D Center (KCRC) grant funded by the Korean government (Ministry of Science, ICT & Future Planning) (2012M1A8A1056408). This research was supported by a National Research Foundation of Korea (NRF) grant funded by the Korean government (MEST) (2012R1A1B3000992).

REFERENCES

(1) Centi, G.; Quadrelli, E. A.; Perathoner, S. *Energy Environ. Sci.* **2013**, *6*, 1711−1731.

(2) Trainham, J. A.; Newman, J.; Bonino, C. A.; Hoertz, P. G.; Akunuri, N. *Curr. Opin. Chem. Eng.* **2012**, *1*, 204−210.

(3) Hu, B.; Guild, C.; Suib, S. L. *Journal of CO_2 Utilization* **2013**, *1*, 18−27.

(4) Centi, G.; Perathoner, S. *Catal. Today* **2009**, *148*, 191−205.

(5) Park, S. W.; Joo, O. S.; Jung, K. D.; Kim, H.; Han, S. H. *Appl. Catal., A* **2001**, *211*, 81−90.

(6) Chen, C.-S.; Cheng, W.-H.; Lin, S.-S. *Appl. Catal., A* **2004**, *257*, 97−106.

(7) Goguet, A.; Meunier, F. C.; Tibiletti, D.; Breen, J. P.; Burch, R. *J. Phys. Chem. B* **2004**, *108*, 20240−20246.

(8) Oshima, K.; Shinagawa, T.; Nogami, Y.; Manabe, R.; Ogo, S.; Sekine, Y. *Catal. Today* **2013**, DOI: 10.1016/j.cattod.2013.11.035.

(9) Ertl, G.; Knötzinger, H.; Schuth, F.; Weitcamp, J. *Handbook of heterogeneous catalysis*; VCH Publishers: Wienheim, Germany, 2007.

(10) Vernoux, P.; Lizarraga, L.; Tsampas, M. N.; Sapountzi, F. M.; De Lucas-Consuegra, A.; Valverde, J. L.; Souentie, S.; Vayenas, C. G.; Tsiplakides, D.; Balomenou, S.; Baranova, E. A. *Chem. Rev.* **2013**, *113*, 8192−8260.

(11) Vayenas, C. G.; Bebelis, S.; Pliangos, C.; Brosda, S.; Tsiplakides, D. *Electrochemical Activation of Catalysis: Promotion, Electrochemical Promotion and Metal-Support Interactions*; Kluwer Academic/Plenum Publishers: New York, 2001.

(12) Vayenas, C. G.; Koutsodontis, C. G. *J. Chem. Phys.* **2008**, *128*, 182506−182513.

(13) Masaki, H.; Masui, T.; Imanaka, N. *J. Alloys Compd.* **2008**, *451*, 406−409.

(14) Nitadori, T.; Ichiki, T.; Misono, M. *Bull. Chem. Soc. Jpn.* **1988**, *61*, 621−626.

(15) Jiang, S. P. *J. Mater. Sci.* **2008**, *43*, 6799−6833.

(16) Royer, S.; Alamdari, H.; Duprez, D.; Kaliaguine, S. *Appl. Catal., B* **2005**, *58*, 273−288.

(17) Bhavani, A. G.; Kim, W. Y.; Lee, J. S. *ACS Catal.* **2013**, *3*, 1537−1544.

(18) Saito, Y. U.S. Patent 8540898, 2013.

(19) Frontera, P.; Modafferi, V.; Frusteri, F.; Bonura, G.; Bottari, M.; Siracusano, S.; Antonucci, P. L. *Int. J. Hydrogen Energy* **2010**, *35*, 11661−11668.

(20) Viana, H. D. A. L.; Irvine, J. T. S. *Solid State Ionics* **2007**, *178*, 717−722.

(21) Zuo, C. D.; Dorris, S. E.; Balachandran, U.; Liu, M. L. *Chem. Mater.* **2006**, *18*, 4647−4650.

(22) Tibiletti, D.; de Graaf, E. A. B.; Teh, S. P.; Rothenberg, G.; Farrusseng, D.; Mirodatos, C. *J. Catal.* **2004**, *225*, 489−497.

(23) Andersson, D. A.; Simak, S. I.; Skorodumova, N. V.; Arikosov, I. A.; Johansson, B. *Proc. Natl. Acad. Sci. U.S.A.* **2006**, *103*, 3518−3521.

(24) Tao, S. W.; Irvine, J. T. S. *Adv. Mater.* **2006**, *18*, 1581−1584.

(25) Zuo, C. D.; Zha, S. W.; Liu, M. L.; Hatano, M.; Uchiyama, M. *Adv. Mater.* **2006**, *18*, 3318−3320.

(26) Feng, Z. T.; Postula, W. S.; Erkey, C.; Philip, C. V.; Akgerman, A.; Anthong, R. G. *J. Catal.* **1994**, *148*, 84−90.

(27) Wang, W.; Wang, S. P.; Ma, X. B.; Gong, J. L. *Chem. Soc. Rev.* **2011**, *40*, 3703−3727.

(28) Wang, L.; Zhang, S.; Liu, Y. *J. Rare Earths* **2008**, *26*, 66−70.

(29) Tong, J.; Clark, D.; Bernau, L.; Sanders, M.; O'Hayre, R. *J. Mater. Chem.* **2010**, *20*, 6333−6341.

(30) Moulder, J. F.; Stickle, W. F.; Sobol, P. E.; Bomben, K. D. *Handbook of X-ray Photoelectron Spectroscopy*; Physical Electronics, Inc.: Chanhassen, MN, 1995.

(31) Yao, B. D.; Chan, Y. F.; Wang, N. *Appl. Phys. Lett.* **2002**, *81*, 757−759.